Chemical Physics 396 (2012) 108–115

Contents lists available at SciVerse ScienceDirect

Chemical Physics

journal homepage: www.elsevier.com/locate/chemphys

Energy transfer and relaxation mechanisms in Cytochrome *c*

Cristina Consani, Olivier Bräm, Frank van Mourik, Andrea Cannizzo [1], Majed Chergui *

Laboratoire de Spectroscopie Ultrarapide, ISIC, Ecole Polytechnique Fédérale de Lausanne, CH-1015 Lausanne, Switzerland

ARTICLE INFO

Article history:
Available online 16 September 2011

Keywords:
Cytochrome *c*
Protein dynamics
Tryptophan
Ultrafast
Pump-probe
Ultraviolet–visible

ABSTRACT

Using broadband UV–vis femtosecond transient absorption and fluorescence up-conversion, we investigate the interaction between the haem moiety of ferric and ferrous Horse heart Cytochrome *c* and its single Tryptophan (Trp) residue and the energy dissipation mechanisms upon excitation at various wavelengths in the visible and the UV. Varying the amount of energy deposited in the haem does not affect the relaxation and cooling processes. Differences are observed between the cooling time-scales of the two redox states, which are attributed to different haem–protein couplings. While energy transfer from the Trp to the haem is observed in the decay of Trp and the response of the haem, excitation of the latter does not induce a clear response of the former. This suggests that for Cytochrome *c*, Trp is not a good marker of the protein response, probably due to its orientation with respect to the haem plane.

1. Introduction

Understanding the signaling through a protein is fundamental for describing its functionality [1]. Among different possible long-range interaction mechanisms, the redistribution of the localized excess of energy generated by biological functions plays an important role, as it induces conformational changes of the entire protein [2].

Optical methods offer a clean way to deposit a controlled amount of energy on a specific protein site and to monitor the following processes. The occurrence of global protein dynamics triggered by localized excess of vibrational energy (EVE) was invoked for haem proteins [2,3], where ligand photolysis by visible light induces a sub-100 fs rise of the haem temperature by up to 300 K [4]. The issue of how, and how fast, energy is redistributed and dissipated in this family of proteins has been widely addressed by experiments [5–7] and molecular dynamics (MD) simulations [4,8–10].

Horse heart Cytochrome *c* (hh Cyt *c*, Cyt *c* in the following) is a relatively small membrane-bound haem protein which plays an important role in many electron transfer processes. Its cofactor is a 6-coordinated iron porphyrin, where the iron is axially bound to a proximal Histidine (His18) and a distal Methionine (Met80). The protein exists in both ferrous and ferric redox states. Upon photoexcitation, the ferrous state undergoes Met80 detachment, followed by a fast biphasic recombination on time scales of 5 and 16 ps. On the contrary, no signatures of photodissociation have been observed in the ferric state [5]. Cyt *c* contains a single Tryptophan residue at 9 Å from the haem and its fluorescence is strongly quenched by Fluorescence Resonance Energy Transfer (FRET) to the haem group [11,12]. The center of mass of the Trp is located almost in the plane of the porphyrin and its indole plane forms an angle of ~70°–80° with the latter.

Cyt *c* is a very promising system to investigate energy redistribution in proteins, since molecular dynamics (MD) simulations have pointed to a very weak influence of the solvent on the energy relaxation [13]. In fact, in contrast to other hemoproteins such as Myoglobin, where the cofactor is almost in contact with the solvent, the haem-pocket of Cyt *c* is buried well inside the protein. The thermal bath of the cofactor is therefore the protein itself. MD simulations determined the Cyt *c* thermal relaxation to be mono-exponential on a ~7 ps time scale, independent of the redox states [13]. Time-resolved resonance Raman (TR^3) results showed instead a two-phase peak position shift of the ν_4^* band in both compounds, on a sub-2 ps and a ~7 ps time scales [5]. These results speak for a more complex temperature relaxation of the haem. Moreover, the authors suggested that the time scales of the intramolecular vibrational energy redistribution are longer in the ferrous moiety, which they attributed to the haem doming induced by Met80 photolysis. The 7 ps temperature relaxation does not appear in transient absorption measurements in the visible range, while pump-probe studies on the two redox species reported different cooling time scales, generally longer for the ferric form [3,5,14]. The extent to which the cooling time scales are affected by the excess of vibrational energy is still not clarified.

The use of naturally occurring amino acids (Tryptophan, Tyrosine), which absorb below 300 nm, as probes of local protein dynamics has been demonstrated both in ultrafast transient absorption measurements of retinal [15,16] and haem proteins

* Corresponding author. Tel.: +41 021 6930457; fax: +41 021 6930365.
E-mail address: Majed.chergui@epfl.ch (M. Chergui).
[1] Present address: Institute of Applied Physics, University of Bern, Silderstr. 5, CH-3012 Bern, Switzerland.

0301-0104/$ - see front matter © 2011 Elsevier B.V. All rights reserved.
doi:10.1016/j.chemphys.2011.09.002

[3], as well as in ps UV-resonance Raman experiments on retinal [17,18] and haem [19] proteins. Dartigalongue et al. [20] also performed ultrafast transient absorption and circular dichroism (CD) on Mb-CO in the 220–360 nm region, concluding that the time-resolved response is mainly due to the haem, while the amino-acids do not contribute significantly. On the other hand, they reported a strong CD change at 230 nm, which they suggested may be due to a transient deformation of the α-helices in the protein. Zhong and co-workers [3] also reported a possible global conformational dynamics following dissociation of the ligand in ferrous Cyt *c*.

Here we report on UV–Vis pump/white-light probe transient absorption measurements of ferric and ferrous Cyt *c* excited at 530 nm and 288 nm. In the former case the lowest haem optical transition (the so-called Q band) is accessed, while the latter corresponds to excitation of both the porphyrin and the Trp. The main novelties of our approach are: (i) we use an ultra-broadband fs probe covering the 670–270 nm range, thus accessing both the Trp absorption [21] and the less exploited porphyrin related absorption transitions [22–25]; (ii) by moving the excitation from 530 nm to 400 nm and to 288 nm, almost 1.2 and 2 eV, respectively, of additional EVE are deposited impulsively in the haem group [26] which, according to the MD simulations [4,13], correspond to a temperature increase of up to ~400 K; (iii) the comparison of the two redox states allows us to disentangle cooling from structural ligand detachment dynamics.

2. Experimental methods

2.1. Sample preparation

Horse heart Cyt *c* was purchased from Sigma Aldrich. The compound was dissolved without any further purification in pH 7 phosphate buffer (30 mM/l KH_2PO_4 + NaOH). No oxidant was added to the solution with ferric Cyt *c*. Ferrous Cyt *c* was prepared by reduction of ferric Cyt *c* in pH 7 buffer by addiction of sodium dithionite ($Na_2S_2O_4$). The salt was then removed by means of gel-filtration desalting columns. Static UV–visible absorption (see Fig. 1) was used to estimate the content of the two redox states and the quality of the sample before and after the measurements. In this way we verified the almost unitary content of the desired state and a negligible content of photo-damaged molecules after laser exposure.

For TA measurements, the concentration of all the samples was adjusted to 0.39 OD at 290 nm in a 0.5 mm cell when probing in the UV, corresponding to a concentration of 0.41 mM. When probing in the visible range, the concentration was reduced to ~0.29 mM. For the visible pump – visible probe experiments on the ferric sample, the concentration was further reduced to ~0.10 mM.

2.2. Transient absorption setup

The experimental setup was already described elsewhere [27]. Briefly, the output of a Regenerative Amplifier (typically 650 μJ at 1 kHz) is used to pump two home-made NOPAs, which produce tunable broadband visible pulses in the range 500–750 nm with a typical length of 40 fs. One of the NOPAs is used to produce either the 530 ± 20 nm broadband pump beam or the UV 288 nm pulse after frequency doubling in a 250 μm β-BBO crystal. The other NOPA is used to produce the broadband UV probe pulse through achromatic doubling in a 150 μm β-BBO crystal. The visible probe is obtained through continuum generation by focusing the 800 nm pulse in a CaF_2 crystal. The pump and probe beams are typically focused into 110 and 90 μm diameter spots, respectively, at the sample position. Typical pump energies are 130 nJ for UV excitation and 160 nJ for visible excitation. The sample was circulated in a 0.5 mm thick UV-grade quartz cell to avoid photo-damage; the flow speed was adjusted to have refresh the sample after each excitation pulse, to avoid re-excitations of the same molecules or heating effects. The pump-probe cross-correlation time, estimated from cross-phase modulation measurements in pure water, was ~160 fs.

The TA signal at each delay time are calculated accordingly to the formula

$$\Delta A = 2 \ln\left(\frac{S_p - S_u}{S_p + S_u}\right) \quad (1)$$

where S_p and S_u are the spectra of the pumped and unpumped sample, respectively. The polarization of the pump with respect to the probe pulse was controlled with a half-wave plate and was set at magic angle (MA).

The TA signals in the spectral region between 400 and 420 nm are distorted because of the high optical density (OD) of the sample. Indeed, when the sample content is adjusted to have a typical value of 0.3–0.4 OD at the pump wavelength, the optical density in the Soret band region (see Fig. 1 and next paragraph) is 1.5 or more. This causes ⩾95% of the probe photons to be absorbed and the TA signal is thus calculated on a small number of counts on the detector. In this situation, small unavoidable contamination due to scattered light, usually negligible, increases the amplitude

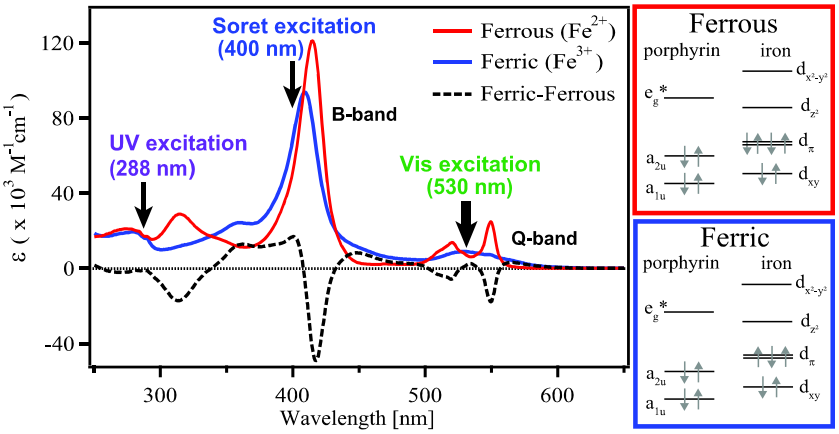

Fig. 1. Static electronic absorption spectra of ferrous and ferric forms of Cyt *c*. Arrows show the pump wavelengths used here. The difference spectrum of the ferric minus the ferrous form is shown as a dashed line. The panels on the right show a qualitative sketch of the ground state orbitals and their occupancy for ferrous and ferric Cyt *c*.

of the denominator in Eq. (1) and reduces the total amplitude of the TA signal. A decrease of the sample concentration (i.e. the OD in the Soret region) permits to partially recover the amplitude of the Soret band bleaching, but decreases the amplitude of the signal in all the other spectral regions, strongly degrading the signal-to-noise ratio. The kinetic and spectral evolution of the Soret region have been exhaustively studied by TA [3,5,14]. For the purposes of this study we were interested in following the complete spectral evolution of the sample on the entire UV–visible range, thus we preferred to adjust the concentration to the best signal-to-noise ratio in all the spectral regions, bearing in mind that the amplitude of the bleaching signal between 400 and 420 nm is underestimated.

2.3. Data analysis

Data were corrected for the group velocity dispersion (GVD). Since the cross-phase-modulation signal in the pure solvent is very strong, especially in the UV region, the first 160–180 fs have been removed from the analysis.

Data matrices have been analyzed by means of a singular value decomposition (SVD) algorithm to obtain the characteristic time scales of the global dynamics and their decay associated spectra (DAS). The reliability of the analysis has been confirmed by a global fit (GF) on 30 kinetic traces at different wavelengths over the entire spectrum. For a more detailed discussion on SVD analysis, refer to [28].

All the data sets we present here have been scaled with respect to the concentration and the photon densities. The absolute values correspond to the 0.41 mM sample excited by 120 ± 10 nJ pulse focused on a spot of ~100 μm diameter.

3. Results

Fig. 1 shows the static electronic absorption spectra of the ferrous and ferric Cyt *c*. The main features of these spectra are the bands at 500–550 nm (Q band), at 405–415 nm (B or Soret band), at 310–370 nm (N band) and <290 nm (L band), which are all related to intra-porphyrin transitions of the haem group [29–31]. Below 300 nm the absorption bands of Trp and of other aromatic amino acids are also present and partially obscure the haem L band [21]. From the known absorption coefficients [32,33], we estimate that ~30% of the absorption at 288 nm is due to tryptophan and ~70% to the haem [30].

Fig. 2 shows TA spectra at magic angle (MA) of ferrous and ferric Cyt *c* in water in the range 270–700 nm, upon excitation at 288 nm and 530 nm. In the latter case the broad spectral width of the pump pulse prevented us from probing the Q band region. The data in the Soret and Q-band region agree well with previous reports (see also Supplementary Fig. SI.1) [5,14,34]. The negative signal at 400–420 nm is due to a bleaching of the Soret band maximum and should be the dominant contribution (see static absorption spectra). However, as mentioned above (see Materials and methods), the high optical density of the sample in this region distorts the amplitude of the difference signal. To our knowledge only one study addressed early fs–ps dynamics in the UV range down to 340 nm for ferric Cyt *c* [34]. Despite the very different experimental conditions in that work (excitation wavelengths of 400 and 266 nm and much higher pump powers, typically 6–13 mJ/cm^2), our data show a good agreement with the reported spectra.

In spite of a complex overall behavior, we identify some general trends: (i) regardless of the sample and the pump wavelength, all the dynamics are over within a few tens of ps; (ii) important narrowing and shifting of the transient bands are observed on a ps time scale above 420 nm; (iii) the main spectral differences in the TA spectra between the two redox forms lie in the 300–350 nm and in the Q band region, and correlate to the different positions of the N-bands in the two redox forms [22] and to the different shapes of the Q-bands; (iv) when changing the excitation from visible to UV, the bands appear generally broader but no new features appear.

In order to analyze the complex behavior in Fig. 2, we carried out an SVD analysis. In Fig. 3 the dominant spectral components for ferrous and ferric Cyt *c* under UV excitation are reported. The long lived (≫200 ps) component is omitted for the sake of clarity. The complete set of DAS for all the samples is available in the SI (Supplementary Fig. SI.2). The extracted time constants are reported in Table 1 and their assignment is discussed below. The major difference between the spectra obtained with visible and UV excitation is observed in the ferrous sample below 290 nm. Here the bleach observed upon visible excitation, which recovers with 5 ps and 12 ps time constants, is not observed when the sample is excited in the UV. Conversely, upon UV excitation a positive (excited state absorption) signal decaying with ~2 ps time constant is obtained (Fig. 4). Fig. 5 compares the TA spectra of ferrous Cyt *c* upon UV and visible excitation before the excess of vibrational energy localized on the haem is completely dissipated. A striking difference appears between the visible bands, strongly broader upon UV excitation, and the negative band at 310 nm, which is almost not affected by spectral evolution.

4. Assignments

We divided the observed dynamics in five groups:

4.1. Excited state decay (τ_{ESD})

According to our recent ultrafast fluorescence measurements, the excited state lifetime of the haem in Cyt *c* is 150–200 fs for both the ferric and ferrous forms [26]. For all the investigated samples the respective DAS shapes present very similar common features (see also the inset in Fig. 3b): (i) an excited state absorption band (positive feature) below 360 nm; (ii) a negative band around 400 nm (where some spectral distortion is present, as discussed in the experimental section); (iii) an excited state absorption band at 455–465 nm. In addition, in the ferrous sample under visible excitation, the DAS associated to the 150 fs time scale contains a dominant spectral contribution that appears as a mirror image of the 6 ps DAS. Both observations are discussed in more details in the next section.

4.2. Trp related dynamics (τ_{Trp}, present only under UV pump)

The ultrafast fluorescence measurements upon UV excitation show that Trp in Cyt *c* decays on a time constant of 350 fs and 700 fs for the Fe^{2+} and Fe^{3+} forms, respectively [26]. Therefore the corresponding time scales reported in Table 1 are attributed to the decay of excited Trp. As expected, these components are obviously missing upon visible excitation.

4.3. Axial ligand recombination (τ_R, present in the ferrous form only)

The DAS at $\lambda > 400$ nm agrees well with previous studies on photo-dissociated ferrous Cyt *c*, where similar kinetics were observed for 400 and 550 nm excitation and were assigned to the transition from the 5-coordinated to the 6-coordinated haem [3,5,14]. As confirmed by these studies and discussed in detail in the next section, the static visible absorption spectra of the 5-coordinated ferrous ($5cFe^{2+}$) haem and 6-coordinated ($6cFe^{3+}$) ferric form are quite similar (Fig. 6). This similarity occurs also in the UV region where the shape of the τ_R DAS in the 290–380 nm range

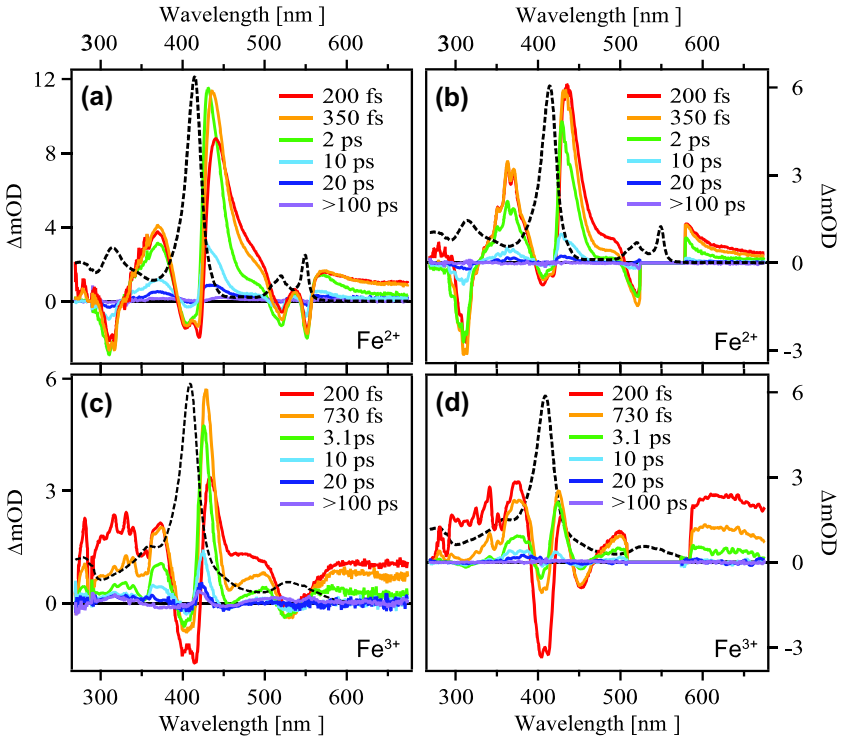

Fig. 2. Selection of transient absorption spectra at different delay times for ferrous Cyt *c* under (a) UV (288 nm) and (b) visible (530 nm) excitation and for ferric Cyt *c* under (c) UV and (d) visible excitation. In each data set, the dashed line represents the ground state absorption spectrum in arbitrary units. Data points close to the pump wavelength are not shown due to distortion.

agrees well with the difference spectrum of the ferrous and ferric absorption in Fig. 1. In particular, the negative band at 310 nm shows a rather simple decay with almost no spectral evolution (Figs. 2 and 5). As it is almost insensitive to cooling phenomena, this band is more suitable to probe recombination than the bands in the visible. In the following we will refer to it as the *recombination band*.

The results under UV excitation are good enough to distinguish a bimodal recombination with ~5 and ~12 ps time constants and with amplitudes of 90% and 10%, respectively, of the total signal. The assignment of this feature is straightforward as we observe that the shape of the related DAS are very similar and do not show cooling features (broadening or shifting of bands). The observation of a biphasic recombination was already reported for Q-band excitation [5]. The authors explained the presence of a longer recombination time in terms of a small percentage of proteins where the methionine–haem mutual orientation after the detachment is unfavorable for the rebinding, and some additional time is needed to achieve a proper steric arrangement.

The most prominent features expected for a 5-coordinated ferric Cyt *c* are the blue-shift of the Soret band from 409 nm to 398 nm and the appearance of two new bands at 500 and 625 nm, as reported previously at pH 0.3 [35]. Our measurements on ferric Cyt *c* do not show any of these features. We thus exclude photodissociation in ferric Cyt *c* on time scales longer than 200 fs, confirming previous results [5].

4.4. Cooling (τ_C)

From a careful comparison of the time dependent spectra (Fig. 2) and the DAS, we deduce that the spectral evolutions of these components (Table 1) consists of mainly narrowing and shifts of bands, which are typical manifestations of a cooling process. From the previous sections, we know that after 220 fs ferric Cyt *c* is in a hot ground state. The absorption bands observed in Fig. 3 between 310–385 nm, 415–448 nm, 466–500 and $\lambda > 587$ nm are due to the broadening and shifting of the N-, B- and Q-bands, respectively. The DAS corresponding to the 3 ps and 11 ps components represent these spectral evolutions. The 700 fs component detected upon visible excitation originates from cooling, which manifests itself mainly by a blue shift of the Soret band. In ferrous Cyt *c*, the 1.8 ps time scale describes a blue shift, as well as an important narrowing, of the Soret-band region absorption, and a small blue shift of the photoproduct Q-band. A minor blue-shift is also observed for the recombination band [36].

For both redox states, we observe sub-ps cooling upon visible excitation. Despite the absence of clear signatures of such evolutions for UV excitation, we cannot exclude a small contribution mixed with the Trp-related signal, since they occur on almost the same time scale.

Comparison with the literature yields good agreement with previously reported cooling times [3,5,14]. In ferric Cyt *c* we find an additional cooling time of 11 ps. A similar decay time at 530 nm was reported and was attributed to a final conformational relaxation of the protein [3]. Thanks to our broad detection window, we could monitor the entire spectral evolution associated to this kinetics, observing that it does contain an important contribution from narrowing and blue-shifting of the Soret band.

4.5. Photoredox Fe(II) ↔ Fe(III) conversion (τ_{PRD})

It has been reported that irradiation by light induces a small percentage of $Fe^{2+} \leftrightarrow Fe^{3+}$ conversion in Cyt *c* [34,37,38]. In all the investigated samples we detect a small long-lived contribution. The good agreement of its transient spectrum with the difference spectrum between the static absorption of the two redox forms in Fig. 1 (except in the Soret band region due to distortion) allows

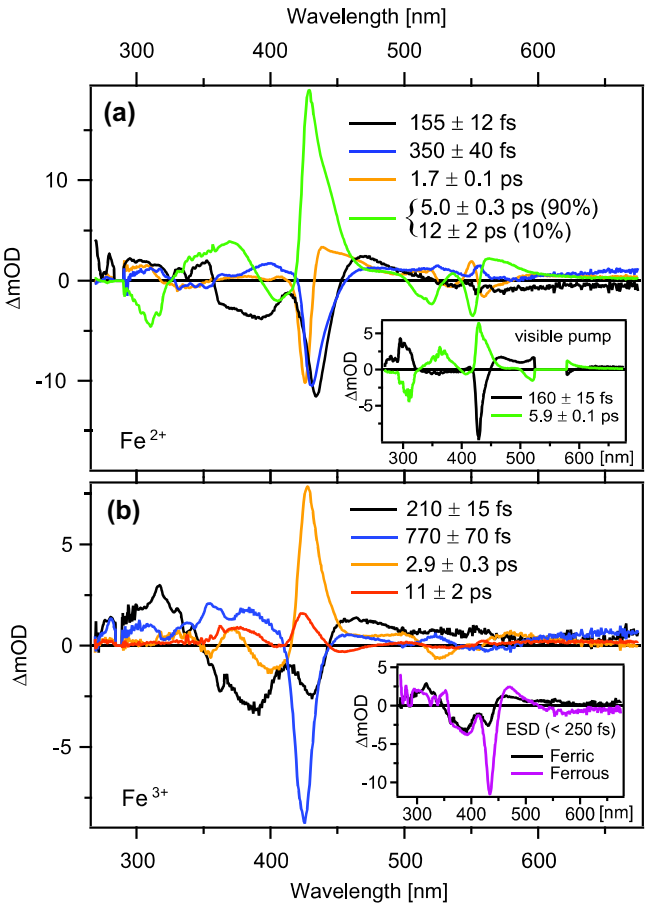

Fig. 3. Decay associated spectra (DAS) for ferrous (a) and ferric (b) Cyt *c* upon UV excitation. For the ferrous sample, the DAS associated to the Met80 recombination process (5 ps and 12 ps components) were combined, having the same spectral shape. For the sake of clarity, the long lived component (≫200 ps) was omitted in both panels. The inset of panel (a) contains the DAS of ferrous Cyt *c* upon visible excitation related to the Excited State Decay (ESD, 160 fs) and to the recombination (5.9 ps) processes. The inset in panel (b) just compares the ESD contributions of the ferrous and ferric Cyt *c* upon UV excitation.

Table 1
Time constants from the SVD analysis of the data in Fig. 2. The respective DAS are shown in Fig. 3 and in Supplementary Fig. SI.2. Reported values are the average of SVD and GF analysis; uncertainty corresponds to a standard deviation.

	Ferrous		Ferric	
	UV	Visible	UV	Visible
τ_{ESD}	155 ± 12 fs	160 ± 15 fs	210 ± 15 fs	220 ± 20 fs
τ_{TRP}	350 ± 40 fs	–	770 ± 60 fs	–
τ'_C	–	600 ± 70 fs	–	700 ± 90 fs
τ''_C	1.7 ± 0.1 ps	1.8 ± 0.5 ps	2.9 ± 0.3 ps	3.4 ± 0.3 ps
τ'''_C	–	–	11 ± 2 ps	11 ± 2 ps
τ'_R	5.0 ± 0.3 ps	5.9 ± 0.1 ps[a]	–	–
τ''_R	12 ± 2 ps	–	–	–
τ_{PRD}	500 ps (fixed)	500 ps (fixed)	500 ps (fixed)	500 ps (fixed)

[a] The data can be fit with equivalent quality with two components of 5 and 12 ps.

us to assign it to a photo-induced conversion between the two forms. The mechanism is not completely understood, but in a recent work Kovalenko and co-workers [34] pointed out the thermal origin of the electron transfer process, which takes place from the electronic ground state. Our results, which show that the effect is stronger upon UV excitation, support their conclusion. Due to the limited range of investigated delay times, this is the "infinity" component which describes all the processes occurring on ns or longer time scales.

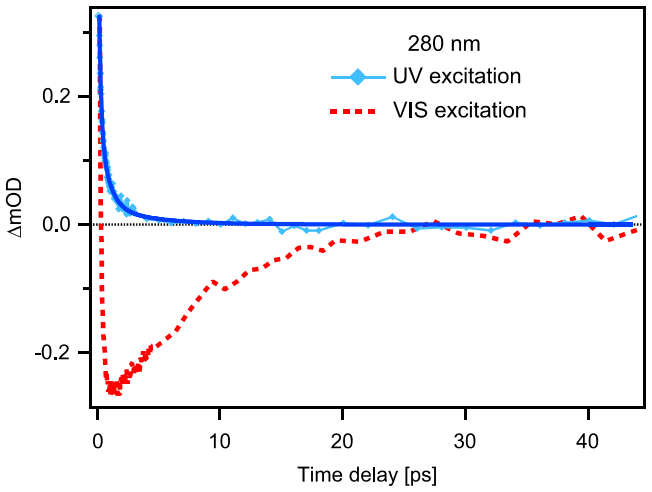

Fig. 4. Transient kinetics in ferrous Cyt *c* at 280 nm upon UV (solid line) and visible (dashed line) excitation. The bleach observed in the latter, a feature characteristic of the photolysis, is not observed when the sample is excited in the UV.

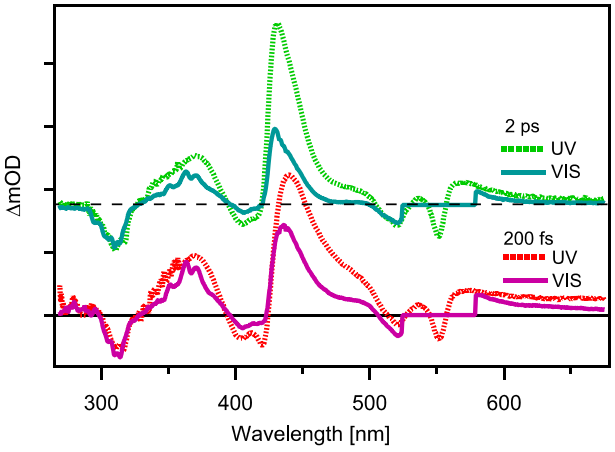

Fig. 5. Comparison of TA spectra in ferrous Cyt *c* under UV and visible (VIS) pump at different times. The traces at 2 ps time delay are vertically shifted for purpose of clarity.

5. Discussion

In the following we discuss in detail the photophysics of the two redox states after the fast electronic relaxation, and the differences in the cooling processes for the two redox states and for the various excitation energies.

5.1. Excited state absorption features and ground state recovery

As stated in the previous section, we attribute the 150–200 fs time scale to the recovery of the porphyrin ground state. In this respect, the associated DAS contains two main contributions: the ground state bleaching and the absorption from electronically excited states. The similarities for different pump energies in the entire spectral range of the DAS in ferric Cyt *c* corroborate this assignment.

The similarity of the sub-200 fs DAS of ferric Cyt *c* with that of the ferrous UV excited sample, shown in the inset of Fig. 3b, is also of interest in this context. The N and L transitions have the same LUMO as the Q and Soret [22]. The following evolution is

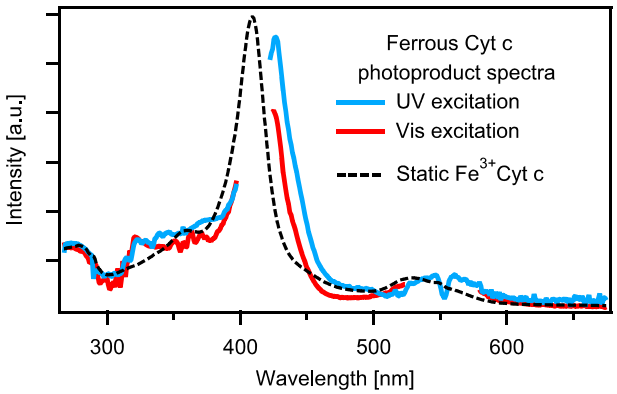

Fig. 6. Photoproduct absorption spectrum reconstructed from the 6 ps spectra upon UV (blue curve) and visible (red curve) excitation by subtraction of the bleaching contribution. In the visible spectrum the region between 520 and 575 nm is removed because of the pump scattering. The wavelength range between 400 and 422 nm is also removed because it is distorted by the high OD of the sample (see also discussion in the text). The UV spectrum is generally broader than the visible one, pointing to the increase of the haem temperature. Note the general similarity of the photoproduct spectral shape with the static absorption of ferric Cyt *c* in the entire spectral range, even if the main Q- and B- band result more red-shifted.

dominated by the Ligand-To-Metal-Charge-Transfer (LMCT) to Fe d states. In the ferrous sample, the metal centered orbital involved in the process is the anti-bonding d_{z^2}, from which photolysis takes place. Ferric Cyt *c*, instead, has a hole in the lower lying bonding d_{Π} orbital [39]. We believe that the ultrafast LMCT in ferric Cyt *c* occurs towards the d_{Π} orbital, thus explaining the lack of Met80 dissociation in this system [26]. Since the Fe excited configurations for the two redox states are different, the striking similarities between the spectral shape of the excited state absorptions over such a wide spectral range must originate from the hole in the HOMO of the porphyrin. We recently showed that the LMCT occurs in parallel with an ultrafast (<40 fs) internal conversion (IC) from the high energy porphyrin singlet excited state S_n to S_1 (the Q-band), and that the excited states relax to the Fe d-orbital manifold with a time constant shorter than the ground state recovery [26]. Thus on a time scale of 150–200 fs, we do expect an analogous porphyrin electronic configuration for the two redox states regardless of the excitation wavelength. We then associate this time scale to the recovery of the porphyrin electronic ground state via back-electron-transfer from the Fe *d* manifold.

The case of ferrous Cyt *c* under Q-band excitation is particularly interesting. Indeed, as seen from the inset in Fig. 3a, its DAS is dominated by a component that appears as a rise of the photoproduct signal (τ_R), speaking for Met80 photodissociation on a 150 fs time scale. On the contrary, when the sample is excited in the UV the rise of the photoproduct signal is much less evident on this time scale, confirming that the major channel for photodissociation occurs from higher porphyrin excited states on a much faster time scale [14]. These results are consistent with a substantially different photolysis mechanism depending on the excited state. This topic is further explored elsewhere [26].

5.2. Methionine photolysis in Cyt c and photoproduct absorption

Our measurements in the visible range are in good agreement with previous studies [5,14] and confirm Met-80 photolysis in ferrous Cyt *c*, both upon UV and Q-band excitation. Interestingly, at any wavelength in this spectral region we find an excellent agreement between the late TA spectra in Fig. 2 (when the cooling is already completed), and the difference between the static absorption spectra of the ferric and ferrous redox species depicted in Fig. 1 (the amplitude mismatch in the 400–420 nm region is due to the spectral distortion previously described). As the observed optical transitions involve several electronic states of the porphyrin ring [31], such a good correspondence over such a broad region can hardly be accidental. Rather, it speaks for a similar electronic structure of the 5-coordinated (5c) ferrous and the 6-coordinated (6c) ferric Cyt *c*, both in terms of orbital occupancy and spatial charge distribution.

On the other hand, the porphyrin orbital occupancy of the 6-coordinated ferrous ($6cFe^{2+}$) haem is the same as the $5cFe^{2+}$ and of the $6cFe^{3+}$ one. Considering that the porphyrin optical bands, Q and B bands in the first place, originate from accidentally degenerate orbitals, ground state wavefunction, as well the higher excited state ones, can dramatically change in shape and character upon a minor perturbation, because of the break-down of the adiabatic approximation [40]. As a consequence, the strong profile changes of the B and Q bands are more likely due to different charge distributions on the porphyrin macrocycle that break the degeneracy. This agrees with the donor character of the Met80 residual: since the sulfur atom shares a lone-pair with the haem–iron, partially balanced by a back-donation, the net charge on the porphyrin nitrogen atoms is increased with respect to the unbound $5cFe^{2+}$ haem [41]. In this respect the net charge on the ring in the transient $5cFe^{2+}$ haem is expected to be close to the $6cFe^{3+}$, where the electrostatic repulsion of the axial electron is balanced by the higher oxidation state. The importance of the charge density on the ring for the Q and B bands structure is also notable when comparing static absorption measurements on different metalloporphyrins, like e.g. octaethyl- and tetraphenyl-porphyrins, which show a ferrous- and ferric-like nature, respectively, just by perturbing the charge distribution [42,43].

Strong similarities between the transient absorption spectrum of $5cFe^{2+}$ and static absorption of $6cFe^{3+}$ are also expected in the UV range. A comparison between the DAS associated to the ligand recombination and the difference between the static absorption spectra of the ferric and the ferrous state show a good agreement, confirming the occurrence of Met-80 photodissociation. A reconstruction of the photoproduct spectrum, shown in Fig. 6, confirms the similarities with the static absorption of the ferric sample, with the main features slightly red-shifted. In particular, in the photoproduct spectrum the N band shifts from 310 nm to ~360 nm, almost the same position it has in the ferric ground state spectrum. This is the origin of the recombination band.

5.3. Trp-haem energy transfer

Upon 288 nm excitation, both porphyrin and Trp are simultaneously excited in a ratio of 5:2. Fluorescence up-conversion measurements on both oxidation states of Cyt *c* have unambiguously assigned a 350 fs component in ferrous and a 700 fs component in ferric Cyt *c* to Trp emission [26]. These decay times represent a significant shortening of the hydrated Trp lifetime [44], which has been attributed to resonance energy transfer to the haem [11,12].

Indeed, as seen in Fig. 7, our results on ferrous Cyt *c* show that UV excitation yields a rise time of the signal on a 350 fs time scale at wavelengths representative of the recombination process. Furthermore, the DAS corresponding to this time scale (blue[2] curve in Fig. 3a) shows clear signatures of a rise of the photoproduct signal at almost all wavelengths (recombination band, Soret absorption, typical bleach of the Q band peaks). In particular we observe that this rise is 1/3–1/4 of the total signal in the recombination band.

[2] For interpretation of color in Fig. 3, the reader is referred to the web version of this article.

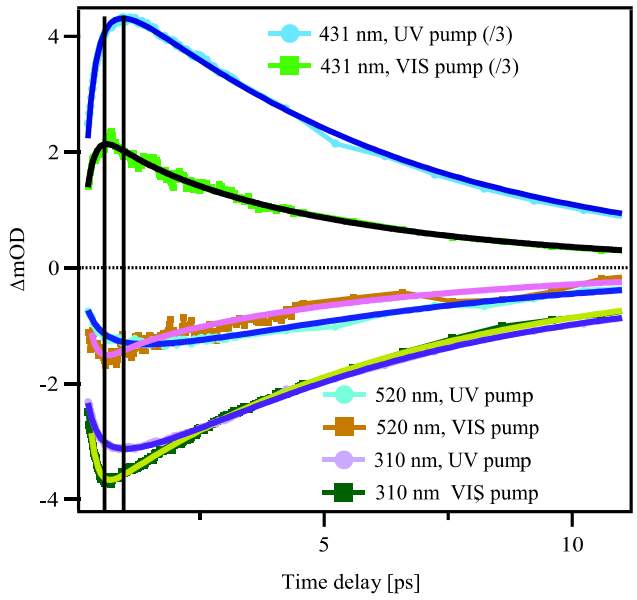

Fig. 7. Comparison between the time traces of ferrous Cyt *c* upon UV and visible excitation in the three characteristic spectral regions of the recombination band (310 nm), low energy shoulder of Soret band (431 nm) and Q-band (520 nm). The vertical solid lines show the maximum signal under the two pump conditions. For UV excitation, the maximum is reached ~350 fs later than for the visible pump.

Since this rise time, which has the same time scale as the Trp deexcitation, is completely missing when the protein is excited in the visible, we conclude that Trp energy transfer to the haem triggers Met-80 detachment. To estimate the quantum yield (QY) for this process, we analyzed the amplitude of the rising component with respect to the total signal of the recombination band. The latter, being almost unaffected by cooling mechanisms, mainly reflects the amount of photolyzed molecules. The ratio between the amplitude of the 350 fs component and the sum of all the slower components in the 300–350 nm region has an average value of −0.26, which correspond to a QY > 85%. A similar result is found analyzing the Q-band region, while unphysical behaviors (QY > 1 or <0) are observed in the Soret-band region, which we ascribe to different cooling mechanisms upon UV or visible excitation: since Trp fluorescence is centered at 350 nm and the internal conversion (IC) and vibrational redistribution (IVR) occur in a few tens of fs [26,45], the haem photoproduct generated by resonance energy transfer is less hot than that directly excited by UV pulses. This is confirmed by the spectra in Fig. 2 and the analysis in Fig. 3: if the energy transfer from the Trp would deliver all the EVE to the haem, haem states completely equivalent to those produced by direct laser excitation would be generated. On the one hand, we have shown that haem cooling occurs on time scales longer than Trp quenching. Thus, the time evolution preceding the cooling would appear as an overall amplitude increase of the haem-related signal without any spectral evolution, which is not the case. On the other hand, for both UV excited ferrous and ferric systems we observe a spectral narrowing already on the Trp time scale (particularly evident in the 450–500 nm range), which confirms the generation of less hot haems. Indeed, as will be discussed in more detail in the next paragraph, an increase of the haem temperature at time zero causes the TA bands to be much broader. This effect is particularly dramatic around the Soret band, which is very intense and narrow. Here a small shift or broadening can cause large differences in the TA spectra, while the same effect is expected to be less pronounced below 350 nm and in the red part of the Q band, where the bands are flatter (see also Supplementary Fig. SI.2).

5.4. Energy dissipation and redistribution mechanisms in Cyt c

Absorption of a 530 nm photon deposits ~54 kcal/mol (2.4 eV) of EVE and ~40 kcal/mol (1.7 eV) in ferric and ferrous Cyt *c*, respectively. For the latter, the Fe-Met80 binding enthalpy has been taken into account [13]. The almost instantaneous internal vibrational redistribution (IVR) and internal conversion (IC) within the haem group increase its temperature by ~200 K [4,8,26]. Upon 288 nm excitation, an additional EVE of 46 kcal/mol (2 eV) is given to the system, causing a further temperature increase of about 200 K.

Comparing our TA results, we notice indeed a much more pronounced band broadening upon UV excitation, while the time scales of cooling are almost unaffected. However, a comparison between the two redox states shows longer cooling times for the ferric system, contrary to previous reports [5,13]. The comparison between visible and UV excitation permits us to exclude that the longer cooling observed in ferric Cyt *c* is due to the larger amount of EVE to dissipate, since the Met80 dissociation energy (~0.6 eV) is significantly smaller than the ~2 eV increase induced by UV excitation. The observed times must be related to a structural difference that affects the haem–protein coupling. Therefore we can definitely rule out the dependence of cooling time scales on the EVE for this system; however, our data cannot distinguish between a static effect due to the different oxidation states and a transient effect caused by ligand detachment as, for instance, haem doming.

Another dissipation mechanism recently proposed for ferrous Cyt *c* is via mechanical waves propagating from the haem group through the protein edifice (*protein-quake*) due to the sudden iron – Met-80 bond breaking [3]. The authors reported a 40 ps bleaching component observed below 300 nm and attributed it to the Trp response to the global deformation of the protein. We did not find kinetic signatures longer than 12 ps, either in TA or anisotropy traces, upon 530 nm and 280 nm excitation. To clarify this discrepancy, we also carried out measurements pumping at 400 nm (see Supplementary Fig. SI.3), which still failed to show such a component in the linear regime of pump powers. The signal-to-noise ratio of these measurements is excellent and leaves no doubts as to the absence of this component. However, different to 530 nm excitation, we observed that the linearity regime is limited to a pump fluence <1 mJ/cm^2, corresponding to 200 nJ on a typical spot of 160 μm diameter. Above this threshold, the TA signal is strongly non-linear and even changes sign at high fluences, transforming from a bleach to an excited state absorption character (see Supplementary Fig. SI.4). Under these conditions we also observed the formation of aggregates on the flow cell windows, even at high flow speed. We additionally performed the same measurement as in Ref. [3] on a sample where the sodium dithionite was not removed, and did not observed differences with respect to the kinetics in the desalinated sample. Overall our results question the occurrence of a 40 ps component in the kinetics [3].

We already pointed out the different character of the signal below 290 nm upon UV and visible excitation in ferrous Cyt *c* (Fig. 4). The excited state absorption contribution detected upon UV excitation has a lifetime that exceeds the Trp energy transfer time. In our fluorescence up-conversion study [26] we did not detect time scales longer than 350 fs in the decay of the Trp, therefore we exclude that this difference comes from the singlet excited state of Trp. This signal, which dominates the bleaching signals of haem and Trp, could be due to a small fraction of the excited Trp's in which an alternative deexcitation pathway takes place, e.g. electron transfer from Trp to the backbone or to the haem [46,47].

We also measured the time-dependent anisotropy of the 288 nm pump/UV–vis probe signals, and found relatively large changes in the wavelength range between 280 nm and 350 nm, which take place on a ps time scale. The anisotropy effect could

indeed be due to the contribution from a transient oxidized Trp specie with a lifetime of ~7 ps. However, the congested nature of this spectral region did not allow us to disentangle the different signals.

6. Conclusions

This study aimed at investigating the coupling between the haem functional center and the Trp residual in Cyt *c*, as well as the energy dissipation mechanisms therein. The spectral range below 360 nm contains indeed a typical feature of the photolysis, which is, contrary to the much more studied Soret band, ideal to disentangle recombination processes from other relaxation mechanisms, since it is scarcely influenced by cooling-related spectral signatures. Monitoring the kinetic evolution in the UV region permitted us to directly probe the Trp-haem resonance energy transfer process, furthermore demonstrating that it induces the Met80 detachment with almost unity QY, just as the direct laser excitation. Despite practically identical photocycles, the two excitation routes are significantly different in the way the EVE is redistributed. In particular, with the excitation via Trp, part of the total EVE (~0.8 eV) is left on the amino acid generating a somewhat colder excited haem than direct excitation. The cooling time scales are characteristic of the protein, and independent of the amount of EVE initially deposited into the haem (in our experiment up to ~100 kcal/mol). This suggests a substantial role of the protein as a cage, aimed at protecting the haem and its functionality. Since the time scale of the relaxation processes is independent of the magnitude of the perturbation, we see no deviation from the linear regime [48].

Neither the photolysis mechanism in ferrous Cyt *c* nor the increase of the EVE induces significant long-lived conformational changes in this protein. The use of the Trp absorption as a local sensor of protein dynamics was demonstrated in bacteriorhodopsin [15,16] and reported also for the same Horse heart Cyt *c* [3] and in several proteins [49–51]. However, in the present work we did not detect a Trp response to haem excitation. Obviously, it could be that Trp in Cyt *c* is not a sensitive probe of structural changes of the protein after excitation. A somewhat similar finding was reported by Dartigalongue et al. in their sub-ps UV transient absorption studies of MbCO [20], but they reported changes in the transient UV CD spectra suggesting a conformational change of the α -helices. However, Mizutani and co-workers reported signatures of structural changes in the ps UV resonance Raman spectra of Trp and Tyr in photoexcited MbCO. They attributed these changes (in particular for Trp14) to the effect of the CO dissociation, as well as a change of environment due to conformational changes in the helices. In MbCO, Trp14 is in the proximal side of the haem and quite exposed to the dissociating ligand, in addition to being in a hydrophobic environment. In Cyt *c*, the Trp amino-acid is almost perpendicular to the haem plane, so that changes affecting the ligand in ferrous Cyt *c* would not have a strong influence on it. In addition, different to MbCO, the relatively rigid linkage of the haem to the protein backbone through the Met80 and His18 residuals limits the effect of bond breaking on the protein structure.

Appendix A. Supplementary data

Supplementary data associated with this article can be found, in the online version, at doi:10.1016/j.chemphys.2011.09.002.

References

[1] C.M. Dobson, Nature 426 (2003) 884.
[2] H. Frauenfelder, B.H. McMahon, R.H. Austin, K. Chu, J.T. Groves, Proc. Natl. Acad. Sci. USA 98 (2001) 2370.
[3] C. Zang, J.A. Stevens, J.J. Link, L.J. Guo, L.J. Wang, D.P. Zhong, J. Am. Chem. Soc. 131 (2009) 2846.
[4] E.R. Henry, W.A. Eaton, R.M. Hochstrasser, Proc. Natl. Acad. Sci. USA 83 (1986) 8982.
[5] M. Negrerie, S. Cianetti, M.H. Vos, J.L. Martin, S.G. Kruglik, J. Phys. Chem. B 110 (2006) 12766.
[6] M. Koyama, S. Neya, Y. Mizutani, Chem. Phys. Lett. 430 (2006) 404.
[7] T. Kitagawa, N. Haruta, Y. Mizutani, Biopolymers 67 (2002) 207.
[8] D.E. Sagnella, J.E. Straub, J. Phys. Chem. B 105 (2001) 7057.
[9] H. Fujisaki, J.E. Straub, Proc. Natl. Acad. Sci. USA 102 (2005) 6726.
[10] M. Devereux, M. Meuwly, J. Chem. Inform. Model. 50 (2010) 349.
[11] S.R. Yeh, S.W. Han, D.L. Rousseau, Acc. Chem. Res. 31 (1998) 727.
[12] Y. Goto, L.J. Calciano, A.L. Fink, Proc. Natl. Acad. Sci. USA 87 (1990) 573.
[13] Y. Zhang, J.E. Straub, J. Phys. Chem. B 113 (2009) 825.
[14] W. Wang, X. Ye, A.A. Demidov, F. Rosca, T. Sjodin, W.X. Cao, M. Sheeran, P.M. Champion, J. Phys. Chem. B 104 (2000) 10789.
[15] S. Schenkl, F. van Mourik, G. van der Zwan, S. Haacke, M. Chergui, Science 309 (2005) 917.
[16] J. Leonard, E. Portuondo-Campa, A. Cannizzo, F. van Mourik, G. van der Zwan, J. Tittor, S. Haacke, M. Chergui, Proc. Natl. Acad. Sci. USA 106 (2009) 7718.
[17] M. Mizuno, M. Shibata, J. Yamada, H. Kandori, Y. Mizutani, J. Phys. Chem. B 113 (2009) 12121.
[18] M. Mizuno, Y. Sudo, M. Homma, Y. Mizutani, Biochemistry 50 (2011) 3170.
[19] A. Sato, Y. Gao, T. Kitagawa, Y. Mizutani, Proc. Natl. Acad. Sci. USA 104 (2007) 9627.
[20] T. Dartigalongue, C. Niezborala, F. Hache, Phys. Chem. Chem. Phys. 9 (2007) 1611.
[21] J.R. Lakowicz, Principles of Fluorescence Spectroscopy, Kluwer Academic/Plenum, New York, 1999.
[22] M. Zerner, M. Gouterma, H. Kobayash, Theor. Chim. Acta 6 (1966) 363.
[23] A.B.J. Parusel, S. Grimme, J. Porphyr. Phthalocya. 5 (2001) 225.
[24] A.B.P. Lever, Iron Porphyrins, Addison-Wesley, Reading, Massachusetts, 1983.
[25] E.J. Baerends, G. Ricciardi, A. Rosa, S.J.A. van Gisbergen, Coord. Chem. Rev. 230 (2002) 5.
[26] O. Bram, C. Consani, A. Cannizzo, M. Chergui, J. Phys. Chem. B doi: 10.1021/jp207615u.
[27] C. Consani, M. Premont-Schwarz, A. ElNahhas, C. Bressler, F. van Mourik, A. Cannizzo, M. Chergui, Angew. Chem. – Int. Ed. 48 (2009) 7184.
[28] I.H.M. van Stokkum, D.S. Larsen, R. van Grondelle, Biochim. Biophys. Acta – Bioenerg. 1657 (2004) 82.
[29] M. Gouterman, J. Mol. Spectrosc. 6 (1961) 138.
[30] W.D. Butt, D. Keilin, Proc. R. Soc. London Ser. B – Biol. Sci. 156 (1962) 429.
[31] M. Gouterman, L.C. Snyder, G.H. Wagniere, J. Mol. Spectrosc. 11 (1963) 108.
[32] H. Edelhoch, Biochemistry 6 (1967) 1948.
[33] H. Kandori, R.F. Borkman, K. Yoshihara, J. Phys. Chem. 97 (1993) 9664.
[34] D. Lowenich, K. Kleinermanns, V. Karunakaran, S.A. Kovalenko, Photochem. Photobiol. 84 (2008) 193.
[35] C. Indiani, G. de Sanctis, F. Neri, H. Santos, G. Smulevich, M. Coletta, Biochemistry 39 (2000) 8234.
[36] J. Rodriguez, C. Kirmaier, D. Holten, J. Chem. Phys. 94 (1991) 6020.
[37] C. Bartocci, A. Maldotti, V. Carassiti, O. Traverso, A. Ferri, Inorg. Chim. Acta – Bioinorg. Chem. 107 (1985) 5.
[38] Y.G. Gu, P.S. Li, J.T. Sage, P.M. Champion, J. Am. Chem. Soc. 115 (1993) 4993.
[39] G. Zoppellaro, T. Teschner, E. Harbitz, V. Schuenemann, S. Karlsen, D.M. Arciero, S. Ciurli, A.X. Trautwein, A.B. Hooper, K.K. Andersson, ChemPhysChem 7 (2006) 1258.
[40] M. Gouterman, J. Chem. Phys. 30 (1959) 1139.
[41] A. Schejter, B. Plotkin, Biochem. J. 255 (1988) 353.
[42] A. Stern, H. Wenderlein, Z. Phys. Chem. Abt. A – Chem. Thermodyn. Kinetik Elektrochem. Eigenschaftslehre 176 (1936) 81.
[43] A. Stern, M. Dezelic, Z. Phys. Chem. Abt. A – Chem. Thermodyn. Kinetik Elektrochem. Eigenschaftslehre 180 (1937) 131.
[44] A.G. Szabo, D.M. Rayner, J. Am. Chem. Soc. 102 (1980) 554.
[45] O. Bram, A.A. Oskouei, A. Tortschanoff, F. van Mourik, M. Madrid, J. Echave, A. Cannizzo, M. Chergui, J. Phys. Chem. A 114 (2010) 9034.
[46] P.R. Callis, T.Q. Liu, J. Phys. Chem. B 108 (2004) 4248.
[47] C. Shih, A.K. Museth, M. Abrahamsson, A.M. Blanco-Rodriguez, A.J. Di Bilio, J. Sudhamsu, B.R. Crane, K.L. Ronayne, M. Towrie, A. Vlcek, J.H. Richards, J.R. Winkler, H.B. Gray, Science 320 (2008) 1760.
[48] N.G.V. Kampen, Stochastic Processes in Physics and Chemistry, North-Holland, Amsterdam, 1981.
[49] L. Zhang, Y.-T. Kao, W. Qiu, L. Wang, D. Zhong, J. Phys. Chem. B 110 (2006) 18907.
[50] W. Qiu, T. Li, L. Zhang, Y. Yang, Y.-T. Kao, L. Wang, D. Zhong, Chem. Phys. 350 (2008) 154.
[51] J.A. Stevens, J.J. Link, Y.-T. Kao, C. Zang, L. Wang, D. Zhong, J. Phys. Chem. B 114 (2010) 1498.